Alexandria Engineering Journal (2023) 75, 261–270

HOSTED BY

Alexandria University

Alexandria Engineering Journal

www.elsevier.com/locate/aej
www.sciencedirect.com

ORIGINAL ARTICLE

Instantaneous torque error compensation based online torque sharing function for Switched reluctance Machines

Ufuk Genc, Burak Tekgun *

College of Engineering, Department of Electrical & Electronics Engineering, Abdullah Gul University, Kayseri, Turkey

Received 1 September 2022; revised 11 March 2023; accepted 27 May 2023
Available online 7 June 2023

KEYWORDS

Switched reluctance machine;
Instantaneous torque error compensation;
Online torque sharing;
Torque ripple minimization

Abstract An online torque sharing function (TSF) with instantaneous torque error compensation method for switched reluctance machines is proposed to maintain a minimized ripple operation. The proposed method adjusts the shared torque between the phases based on instantaneous torque error different than the existing TSF methods formulated with a mathematical expression. The objective of this approach is to benefit from the outgoing phase torque as it has slow current dynamics due to the high inductance. Also, the incoming phase is turned on as soon as it can generate positive torque. During this process, the total torque is estimated instantaneously using lookup tables, and a correction current is calculated and injected into the incoming phase reference current as the inductance is low and current dynamics are fast. This way, the torque ripple is reduced for a wide speed range. Compared to the conventional linear, sinusoidal, exponential, and cubic TSFs, better torque ripple performance is obtained.

1. Introduction

Switched reluctance machine (SRM) is a simple electrical machine as the stator and rotor consist of salient poles where only the stator has windings. Since there is no excitation with magnets and windings in the rotor, these machines are cost-effective, environmental-friendly, and more reliable compared to other motor types. Therefore, it attracts researchers' attention worldwide [1,2]. The control of these machines, however, is more challenging than the DC and AC machines as each phase of the SRM excited consequently with square current waveforms in an independent manner. The main shortcomings of the SRMs are high torque ripple, vibration, and acoustic noise as they have double salient pole structures [3,4].

There is extensive research in the literature for reducing the torque ripple using various control methods. Considering that the major attribution of the torque ripple is due to the commutation between the phases. Compared to the torque production when only one phase is excited, the torque varies abruptly during the commutation region where both two consecutive phases are excited. A well-known strategy is to control the firing angles to obtain a minimum torque ripple[5,6]. Various

* Corresponding author.
E-mail addresses: ufuk.genc@agu.edu.tr (U. Genc), burak.tekgun@agu.edu.tr (B. Tekgun).

Peer review under responsibility of Faculty of Engineering, Alexandria University.

https://doi.org/10.1016/j.aej.2023.05.085

optimization techniques are employed to determine the optimal firing angles that result in minimum torque ripple [7]. Torque control methods are also favored as they make it possible to control the torque during the commutation instants [5]. Torque control methods include direct torque control [8], direct instantaneous torque control [9], current profiling [10], direct flux control [11],and torque sharing function (TSF) [12–22].

TSF is a method where the torque command is shared with the commutating phases in a complementary manner. In this method, the torques generated by consecutive phases are shared in a way that the total torque is equal to the desired value. Usually, the reference torques are generated based on an analytical expression such as sinusoidal, cubic, exponential, etc. The TSF can be obtained or calculated in real-time or in an offline manner.

In [12], an optimization algorithm called the ant colony is used to obtain the optimum firing angles of a cubic TSF through simulations. The turn-off angle and overlapping angle were estimated with respect to the turn-on angle to minimize the computational cost. In [13], the genetic algorithm (GA) is used to calculate the optimal commutation control angles for the linear, cubic, sinusoidal, and exponential TSF. Here, how the copper loss and the torque ripple are varied with respect to the cost weighting factor is investigated. The exponential TSF was determined to be the best method in terms of torque ripple minimization. In [14], an offline TSF that takes phase currents and their derivatives into account during the commutation period is presented. A factor called the Tikhonov factor is calculated for reducing copper loss and the derivation of the flux. In [15], the optimal current profile is determined using the static flux linkage characteristics. In [16], another type of TSF is reported which minimizes the total current during the commutation period. In [17], torque ripple was reduced by introducing a nonlinear modulation that regulates consecutive phases based on the position and outgoing phase current. These phases of regulation are separated in three different ways and selected linear and non-linear functions depending on the saturation, hence, the current tracking error is eliminated. In [18], a dynamic model of the SRM is used to achieve better current tracking. However, a negative torque is generated at each commutation that is compensated by additional positive torque produced by the incoming phase. Although the torque ripple is reduced, the input current is increased as a result of the negative torque compensation, which in turn, causes a higher copper loss. In [19], the Switching period which changes torque error is introduced which is based on a non-linear logical TSF. Here, the base torque generating phase is selected as the incoming phase and the outgoing phase current is adjusted accordingly. However, the incoming phase that has a low inductance cannot produce adequate torque in the extended speed range, which results in an increased torque ripple. In [20], a non-linear TSF with flux linkage controller is reported that takes the saturation into account. In [21], two operation modes are presented with the flux linkage variation of the commutating phases. The torque ripple is reduced, and the SRM can operate at an extended speed range. In [22], two-mode the current control algorithm introduced in [19] is developed by applying the parameters obtained by optimization to an online TSF.

This article presents a TSF method to mitigate the torque ripple in an extended operating range. Unlike the conventional methods, torque sharing is done by cascading the TSF with a dynamic torque error compensator. This way, the torque sharing strategy can be operated beyond the base speed with a significantly reduced torque ripple. Based on the speed and reference steady-state current, the turn-off angle is determined for it to produce the maximum phase torque until it reaches the negative torque region. The incoming phase is energized whenever it can produce a positive torque. The controller instantaneously estimates the output torque using lookup tables (LUT) and compensates the torque error by adjusting the incoming phase current. As the cubic TSF performance superior to the other conventional TSF methods [1], the cubic TSF and the proposed method are compared at various speed conditions. For the low-speed region, a similar performance is observed with the proposed and cubic TSF methods. However, the torque ripple at base speed and above base speed decreased significantly with the proposed method. Torque ripple at the base speed is observed as 27% with the cubic TSF while it is 9% with the proposed method. At above the base speed, the torque ripple reaches 32% with the cubic TSF, while it is 11% with the proposed method.

This paper is organized as follows: Torque control methods and TSF are explained in section 2. In section 3, the proposed TSF method is explained in detail. Simulation and experimental results and discussion are provided in section 4. The paper is finalized in Section 5 with concluding remarks.

2. SRM Control and TSF

2.1. Torque control methods

Torque control methods are categorized as direct and indirect ones based on the feedback data. In the direct torque control, the torque is controlled based on the direct torque estimation feedback, while in the indirect method, it is done by phase current feedback. Direct control methods are classified as direct and direct instantaneous torque control methods. Direct torque control needs two reference inputs torque and flux linkage where the flux linkage is calculated with the voltage and current feedbacks; the torque is calculated with the current and rotor position feedbacks. These two flux-linkage and torque estimations are used to calculate the reference voltage vector to regulate the flux-linkage and torque. However, this method can work at a limited speed. The direct instantaneous torque control method [23] is classified as the current profiling and TSF methods. The current profiling technique essentially determines the reference currents to control the torque. These reference phase currents are determined without using the current vs. position and torque LUT. Hence, TSF is a favorable indirect torque control method as it is simple and has low computational burden. The total torque is shared between the commutating phases.

2.2. Torque sharing function

TSF is the more useful and simple indirect torque control method among others [2]. Due to the nature of the SRM, the total reference torque must be shared with adjacent phases, therefore torque ripple occurs during the commutation period. Fig. 1 illustrates the block diagram of the TSF torque control method for a three-phase SRM.

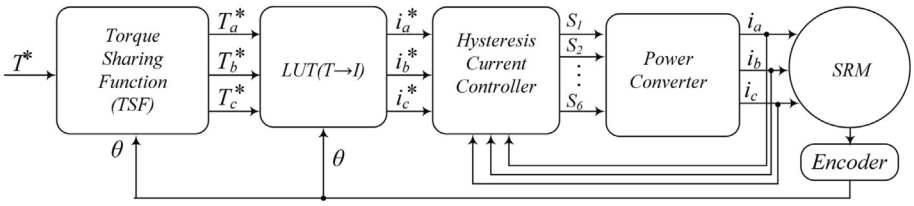

Fig. 1 The block diagram of the TSF torque control method.

To produce ripple-free torque, the reference torque is split into each phase using various distribution functions. The reference torque values for each phase are expressed as follows

$$T_{ref} = \begin{cases} 0 & 0 \leqslant \theta \leqslant \theta_{on} \\ T_{ref} f_{rise}(\theta) & \theta_{on} < \theta < \theta_{on} + \theta_{ov} \\ T_{ref} & \theta_{on} + \theta_{ov} \leqslant \theta < \theta_{off} \\ T_{ref} f_{fall}(\theta) & \theta_{off} \leqslant \theta < \theta_{off} + \theta_{ov} \\ T_{ref} & \theta_{off} + \theta_{ov} \leqslant \theta < \theta_p \end{cases} \quad (1)$$

here, T_{ref}, f_{rise}, and f_{fall} represent the reference torque, rising, and decreasing functions for consecutively triggered phases. θ_{on}, θ_{ov}, and θ_{off}, are represented as turn on, overlap, and turn off-angles, and θ_p is the pole pitch which is defined as follows.

$$\theta_p = \frac{2\pi}{N_r} \quad (2)$$

Here, N_r represents the rotor number of pole.

Reference phase currents are formed using torque to current LUT determined using Finite Element Analysis (FEA). Hysteresis current control is considered as conventional and most preferred in the SRM due to its simplicity.

Conventional TSFs are classified as linear and nonlinear TSF. Non-linear TSFs are classified as cubic, sinusoidal, and exponential TSFs. Conventional methods can be effectively used at low speeds with a minimized torque ripple. However, the torque ripple increases because of the current tracking error at high speeds. Fig. 2.a and 2.b show linear and cubic TSF curves, respectively. Region I and Region III are called the commutation regions where both two consecutive phases are active. In these regions, the reference torque is shared equally between the incoming and outgoing phases. On the other hand, single-phase conduction occurs in Region II.

The linear TSF distributes the torque linearly with the rising and falling functions that can be formulated as

$$\begin{aligned} f_{rise}(\theta) &= \tfrac{1}{\theta_{ov}}(\theta - \theta_{on}) \\ f_{fall}(\theta) &= 1 - f_{rise}(\theta + \theta_{on} - \theta_{off}) \end{aligned} \quad (3)$$

where, the f_{rise} has to ascend from 0 to 1, while the f_{fall} has to descend from 1 to 0 during the commutation. Although the linear TSF is practical, it has a higher torque error because the SRM has a higher nonlinear inductance slope beginning and end of the commutation.

The rising and falling functions of the cubic TSF are expressed as follows.

$$\begin{aligned} f_{rise}(\theta) &= \tfrac{3}{\theta_{ov}^2}(\theta - \theta_{on})^2 - \tfrac{2}{\theta_{ov}^3}(\theta - \theta_{on})^3 \\ f_{fall}(\theta) &= 1 - f_{rise}(\theta + \theta_{on} - \theta_{off}) \end{aligned} \quad (4)$$

The torque generated by the adjacent phases are shared with a cubic function according to the rotor position. This method is better than linear TSF, but cubic TSF will not be sufficient when the SRM inductance characteristic has high nonlinearity.

The rising and falling functions of the sinusoidal TSF [24] are defined as follows.

$$\begin{aligned} f_{rise}(\theta) &= \tfrac{1}{2} - \tfrac{1}{2}\cos\tfrac{\pi}{\theta_{ov}}(\theta - \theta_{ov}) \\ f_{fall}(\theta) &= 1 - f_{rise}(\theta + \theta_{on} - \theta_{off}) \end{aligned} \quad (5)$$

Here the torque is distributed to the adjacent phases with a sinusoidal function.

In the exponential TSF, the rising and falling function of exponential TSF is defined as

$$\begin{aligned} f_{rise}(\theta) &= (1 - \exp(\tfrac{-(\theta-\theta_{on})^2}{\theta_{ov}})) \\ f_{fall}(\theta) &= 1 - f_{rise}(\theta + \theta_{on} - \theta_{off}) \end{aligned} \quad (6)$$

Similar to the other TSF methods, the torque is distributed with an exponential function between the phases based on the rotor position.

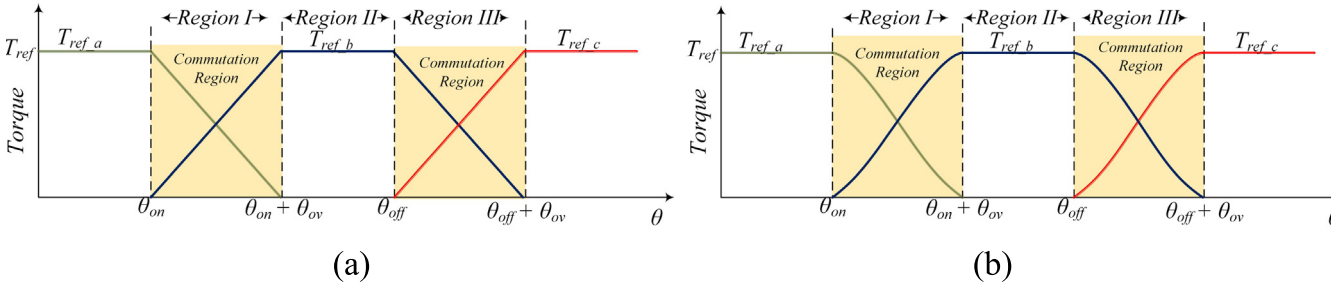

Fig. 2 (a) Linear and cubic TSF functions.

Among the conventional linear, sinusoidal, cubic, and exponential TSF methods, the cubic TSF performs the best [2]. Hence, in this study, the performance comparison is made with conventional cubic TSF.

3. Proposed Adaptive TSF

The proposed TSF method is an online method where the torque sharing is done by cascading the TSF with a dynamic torque error compensator. This way, the torque sharing strategy can be operated beyond the base speed with a significantly reduced torque ripple. Here, the turn-off angle is calculated based on the speed and reference steady-state current. Considering that most of the total torque is produced by the outgoing phase and the rate of change of the current is low due to the high inductance values, it is aimed to benefit from this fact. Hence, it is calculated in a way that when the outgoing phase current reaches to zero, it should not generate a negative torque. However, if the outgoing phase current is brought down to zero using full negative bus voltage, the torque dips down rapidly and the torque produced by the incoming phase current is not enough to track the reference torque. Hence, the outgoing phase current is brought down zero with a second-order filter to provide a smooth current trace. The frequency of the filter is optimized for the minimum torque ripple performance using the parameter sweeping technique. The incoming phase is energized whenever it can produce a positive torque and has the lowest phase inductance. The controller instantaneously estimates the output torque using LUTs and measured phase currents; hence, adjusts the incoming phase current to compensate for the torque error. The details of the control are explained below.

3.1. Control of the outgoing phase

The torque generated in an SRM is expressed as

$$T = \frac{1}{2}\frac{dL(i,\theta)}{d\theta}i^2 \tag{7}$$

In an SRM, the polarity and value of the torque produced are the functions of the rate of change of inductance. In Fig. 3, current and inductance waveforms of an SRM are presented together; where, L_u, L_a, θ_{on}, θ_{off}, and θ_m are unaligned and aligned inductances, the turn-on/off firing angles, and the maximum angle for generating the positive torque for the longest duration, respectively. In the saturation region, the inductance is at its maximum levels, so the torque control is constrained in this region. However, the torque generated from the outgoing phase is higher than it is from the incoming phase in the unsaturated region. Therefore, the turn-off angle of the outgoing phase should be adjusted for producing the maximum torque. But the phase current should not exceed the saturated region as the phase current goes beyond the saturated region, it generates negative torque. Therefore, the angle that the outgoing phase current starts decreasing should be determined carefully. Moreover, when the active phase is turned off at θ_{off}, if a full negative bus voltage is applied, the torque dips down rapidly, and compensating such torque ripple with the incoming phase current becomes challenging. To avoid instantaneously happening torque dip, the outgoing phase reference current is brought down to zero using a 2nd order low-pass filter (LPF).

The 2nd order LPF has a dynamic response that smoothly varies and brings down the reference current to zero. The natural frequency and the damping values of the 2nd order LPF have to be determined as these values define how the current reference varies from its initial value to zero. Also, these values need to be updated based on the speed and initial phase current values.

Fig. 4.a presents the block diagram of the proposed TSF algorithm. Here, steady-state reference currents are obtained via the T-i-θ LUT. This reference current is the value that the current can reach while in single-phase conduction and is represented as I^{SS}_{REF}.

In the commutation block, phase currents are set as a square wave. These phase currents are called raw currents and are represented as I_{a_raw}, I_{b_raw}, and I_{c_raw}. The reference raw phase currents obtained in the output of the filter are symbolized as $I^{ref}_{a\_raw}$, $I^{ref}_{b\_raw}$, $I^{ref}_{c\_raw}$. Fig. 4.b shows the reference raw phase current. In this figure, the turn-off angles at different speeds, θ^{I}_{off}, θ^{II}_{off}, and the settling time of the 2nd order LPF, T^{I}_{s}, T^{II}_{s}, are shown. The settling time, T_s, of the filter is calculated as

$$T_s = \frac{-ln(tolerance\,fraction)}{2\pi\zeta f_n} \tag{8}$$

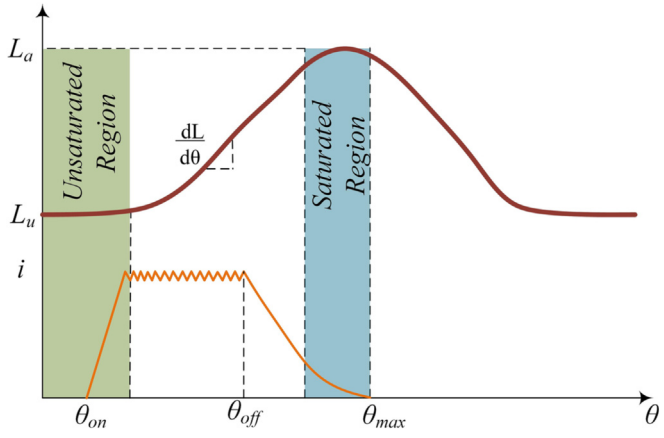

Fig. 3 Inductance and current profile of an SRM.

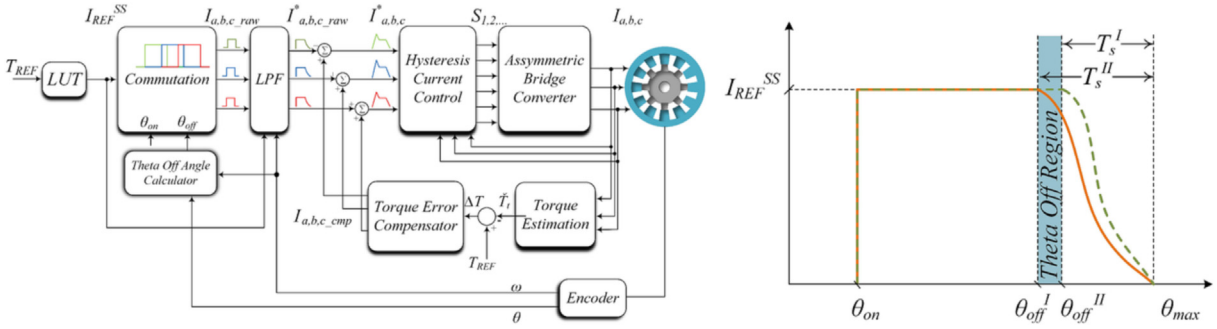

Fig. 4 (a) Block diagram and (b) filtered raw current reference waveform in the proposed method.

where, ζ and f_n represent the filter's damping ratio and natural frequency, respectively. The tolerance fraction is a factor that indicates the error band of the filter. For most underdamped second order filters this value is selected as 0.02. Here, the T_s should be varying based on the speed and the steady-state current; therefore, the natural frequency of the filter will be varying accordingly. The damping ratio and the natural frequency are the parameters that are affecting the turn-off current reference dynamics. To obtain the desired torque ripple performance, these values are optimized for various speed and steady-state current conditions using the parameter sweeping technique. Here the damping ratio is found to be optimal at 0.5 as this value provides a smoother current reference at the beginning of the commutation. After determining the optimal natural frequency values versus the steady state current, I_{REF}^{SS}, and speed, ω, the optimal natural frequency values are curve fit to a second-order polynomial function as

$$f_n = p_{00} + p_{10} \times I_{REF}^{SS} + p_{01} \times \omega + p_{11} \times I_{REF}^{SS} \times \omega + p_{20} \times \left(I_{REF}^{SS}\right)^2 + p_{02} \times \omega^2 \quad (9)$$

where, p_{00}, p_{10}, p_{01}, p_{11}, p_{20}, and p_{02} are the polynomial coefficients which are 13.08, 0.5827, 0.8788, −0.002949, −3.5 94 × 10^{-5}, and −0.8147 × 10^{-7}, respectively.

Once the settling time, which is how long the current takes to go down to zero, is calculated, the settling time is converted to the settling angle by multiplying the speed. Then the turn-off angle is calculated by subtracting the settling angle from the maximum operating angle, θ_{max}. Here, the maximum operating angle is the point where the phase inductance derivative with respect to the rotor position becomes significantly high in the negative direction. In other words, it is the point where the torque generation grows in the negative direction if a current exists in the phase windings. Since the settling time is calculated with speed and steady-state current values, various operating points result in different turn-off angles, which makes the operation adaptive. The tolerance fraction of the LPF and the inductance profile of the SRM are considered when determining the maximum operating angle. Thanks to this method, the negative torque generation at the end of the turned-off phase is eliminated, and better current tracking is achieved.

3.2. Torque error compensator

In the unsaturated region, as the phase inductance is low, the current control dynamics are faster compared to the saturated one. Hence, it is possible to achieve instantaneous torque control by adjusting the incoming phase current dynamically. In the proposed method, the incoming phase filtered raw current reference, $I^*_{a\text{-}b\text{-}c,\ \mathrm{raw}}$ is set to the desired steady-state value to rise the current as soon as it can produce positive torque. However, this raw current reference will not be producing the torque that is complimentary to the outgoing phase torque. Hence, an additional torque compensator is used to compensate for the torque error. For compensation, the instantaneous torque should be either measured or estimated. It is not possible to measure such torques coming from each phase, using an estimator is the viable option. The estimator can be realized through either a mathematical model or LUTs. Considering that the SRM has a highly nonlinear nature, estimating the torque could be a tiresome process with the mathematical model. Hence, a LUT-based torque estimation method is employed to estimate the torques produced by each individual phase and calculate the error. To simulate the SRM in MATLAB / Simulink, two LUTs are generated using the FEA model of the SRM, which are the flux linkage versus the rotor position and current, $\lambda(\theta,i)$ (46-by-81), and torque versus the position and current, $T(\theta,i)$ (46-by-81). In addition to these two LUTs, there is another LUT generated for calculating the current from the given torque and position inputs, $i(\theta,T)$ (109-by-126). The $i(\theta,T)$ LUT has a higher resolution than the other LUTs as the current is highly nonlinear and requires higher resolution for accurate calculation. All estimated torque values are summed and the total estimated torque, $\check{T}_{total}$, is determined. The torque error is calculated using the estimated and reference torques. The torque error compensator block converted this error value into the compensation currents, $I_{a\text{-}cmp}$, $I_{b\text{-}cmp}$, $I_{c\text{-}cmp}$, with the help of the $i(T,\theta)$ LUT. Later these currents are added to the filtered raw reference current waveform and the torque error is eliminated.

In summary, during the commutation, the phase currents are split into two separate torque-sharing control methods. Firstly, the turn-off angle is adjusted adaptively based on the instantaneous speed and reference steady-state current to have the best current tracking performance for the outgoing phase. Secondly, the incoming phase current is adjusted based on the instantaneous torque estimation and torque error. Since the incoming phase inductance value is small, a good current control performance is achieved; hence, the torque ripple is eliminated successfully. Moreover, torque ripple minimization performance at high speed is superior compared to the classical techniques.

4. Result and Discussion

4.1. Simulation results

The SRM parameters considered in this work are presented in Table 1.

FEA of the considered SRM is used to generate the torque-phase current-rotor position *(T-i-θ)*, inductance-phase current-rotor position *(L-i-θ)*, and flux linkage-current-rotor position *(λ-i-θ)* LUTs. Also, the inverse LUTs are generated to be used for estimating the reference currents in the cubic TSF and compensation currents in the torque error compensator.

The simulations are carried out using Matlab© Simulink. The performance of the proposed method and the classical cubic TSF are compared for low speed, base speed, and above base speed. The hysteresis current regulation having a hysteresis band of ± 0.2 A is used with a conventional asymmetric half-bridge converter. The torque waveforms are recorded and torque ripple, T_{ripple}, is calculated as

$$T_{ripple} = \frac{T_{\max} - T_{\min}}{T_{avg}} \tag{10}$$

where T_{max}, T_{min}, and T_{avg} are the maximum, minimum, and average values of the SRM torque. The sampling time is an important aspect of the hysteresis control as longer control periods cause a bigger hysteresis band that causes a higher torque ripple.

Considering the computational speed of the microcontroller, the control period is selected as 12 μs in the experimental studies; hence, the simulation is also operated at 12 μs. In the simulations, using the proposed and conventional cubic TSF methods, the torque ripple, and peak currents are compared. In Fig. 5.a, Fig. 5.b, Fig. 5.c, Fig. 5.d, Fig. 5.e, and Fig. 5.f, the waveforms of the conventional cubic TSF and the proposed method when the motor operates at 400, 1000, and 1200 rpm are shown, respectively. These waveforms indicate phase currents, phase torques, and total torque, respectively.

For the Cubic TSF, firing and overlap, angles are selected as 7.5°, 15°, and 2.5° for all speed levels by manually sweeping their values to eliminate the torque ripple and minimize the RMS input current in the commutation period. In the proposed method, the turn-on angle is set to 7.1° as this angle is the minimum inductance angle where a positive torque can be generated. The turn-off angle is calculated as 15.61°, 15.13°, and 15.05° for 400, 1000, and 1200 rpm speeds, respectively. These values are calculated based on the rotor speed and steady-state phase current values. Fig. 5.a presents the waveforms of the cubic TSF when the motor runs at 400 rpm. The phase currents can track the reference phase currents due to the low absolute Flux derivation values at low speeds; hence, the ripple is observed as 5%. Fig. 5.b presents the simulation result with the proposed TSF at 400 rpm. Compared to the cubic TSF, a similar torque ripple is obtained; however, the cubic TSF phase current is exceeding 20 A, while it reaches 20 A with the proposed method. Hence, despite having a similar torque ripple, the copper loss is higher in the cubic TSF.

Table 1 SRM Specifications.

Nominal power	1.25 kW
Nominal torque	12 Nm
Stator/Rotor pole configuration	24 / 16
Number of phases	3
Base speed	1000 rpm
Rated Voltage	200 Vdc

The waveforms of the cubic TSF at the base speed, 1000 rpm, are provided in Fig. 5.c. The absolute Flux derivation value increases with the speed, as a result, the phase current tracking performance decreases. Hence, the error and the torque ripple increase as illustrated in Fig. 5.d. The ripple at the base speed is observed as 27% while the maximum phase current is recorded as 28 A. The proposed control method varies the turn-off angle with the speed and steady-state phase current to improve the current tracking and torque ripple performance. Hence, the current tracking error is minimized, the torque ripple is brought down to 9%, while the peak phase current is reaching to 22 A.

Simulations are also performed above the base speed at 1200 rpm. The cubic TSF results in 32% torque ripple with a high current tracking error and high peak phase current as shown in Fig. 5.e. However, the torque ripple kept under 11% using the proposed method while having a 23 A phase current which was 28 A in cubic TSF as shown in Fig. 5.d. The current tracking performance is also superior to the cubic TSF when operating at high speed.

According to the simulation results, the proposed method successfully tracks the currents with a small tracking error and acceptable peak currents; hence, the torque error and torque ripple are minimized. It should be noted that eliminating the torque ripple improves the accuracy of the average torque and make it close to the reference value. Higher the ripple during the commutation, the larger the deviation on the average torque value from the reference value. While operating at high speeds, the current tracking error increases; however, keeping it at its minimum level is possible thanks to the adaptive turn-off angle is adjustment. As a result, with the proposed method performed better than the cubic TSF above the base speed.

4.2. Experimental results

To validate the proposed method, a series of experiments are carried out. The specifications of the SRM under test are provided in Table I. The test system includes a dynamometer system that has a loading machine that is driven with a commercial regenerative motor drive unit in speed control mode, a torque transducer, an oscilloscope, current probes, the SRM under test, and its drive unit. The connection diagram of the test system and a photograph of the experimental setup is provided in Fig. 6.a and Fig. 6.b.

The SRM used in this study is designed by one of the authors and reported in previous work [25]. The LUTs used in this work are obtained from the FEA model of the SRM. In the SRM drive unit, an asymmetric bridge converter having SiC MOSFETs is used with the hysteresis current controller. A Texas Instruments TMS320F28379D microcontroller is used to implement the controls with a 12 μs control period. Similar to the simulation studies, a hysteresis current band of 0.2 A is

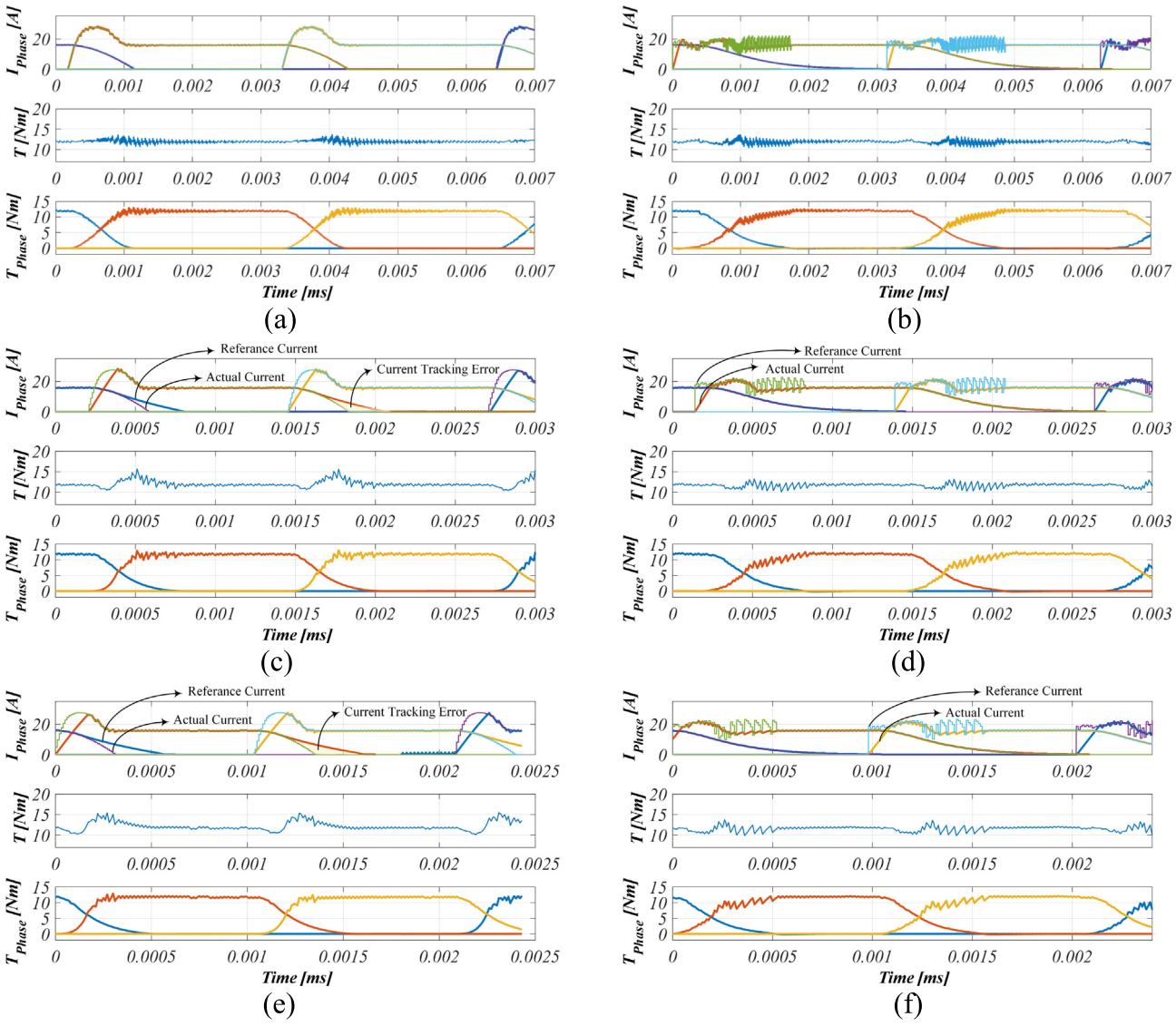

Fig. 5 Simulation results at (a) 400 rpm with Cubic TSF and (b) the proposed method; (c) 1000 rpm with Cubic TSF and (d) proposed method; (e) 1200 rpm with Cubic TSF and (f) the proposed method.

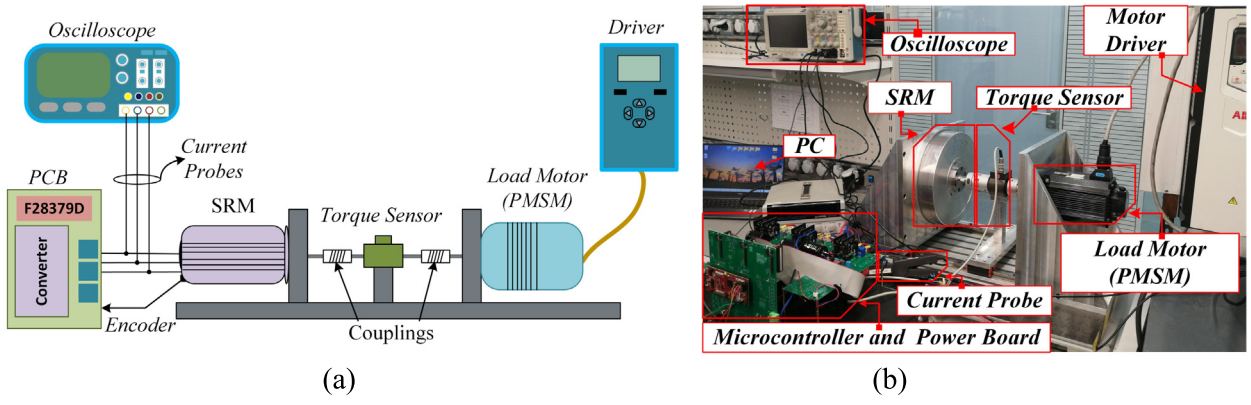

Fig. 6 (a) Block diagram of the test system and (b) experimental setup.

used in the experimental studies. During the tests, the torque control method is used while the dynamometer is rotating at various constant speeds. A 1000-pulse quadrature encoder is used for speed and position feedback. The phase currents are measured with Tektronix A622 current probes, and the torque transducer signal is captured with the voltage probes. These signals are observed in a Tektronix MDO 3014 100 MHz oscilloscope.

Experiments are conducted for the maximum current condition at low, the base, and high speeds. The torque ripple and current waveforms are observed to validate the simulation results. In Fig. 7.a, the currents and torque curves are given when the machine is operated with 16 A at 400 rpm speed. It is observed from the plot that the torque ripple is 8%, the peak current is 16 A, and the average torque is 12 Nm for this condition. Later the experiments are conducted at the base speed, 1000 rpm while commanding the maximum torque. The average torque and the torque ripple are measured as 12 Nm, and 15%, while the peak current is measured as 18.5 A as presented in Fig. 7.b. The experiments are also conducted above the base speed to evaluate the performance at high speeds. The results at 1200 rpm and 1400 rpm are given in Fig. 7.c and Fig. 7.d, respectively. When the machine operates at 1200 rpm, the average torque, the torque ripple, and the peak phase currents are observed as 11.5 Nm, 21%, and 18A; and when it operates at 1400 rpm, these values are measured as 9.5 Nm, 29 % and 17.5 A, respectively.

As the motor speed exceeds the base speed, the outgoing phase current is set to a backward position to prevent the generation of negative torque, which is demanding a faster dynamic response from the current regulator. However, the current regulator bandwidth is limited with the control period, which degrades the current tracking performance on the outgoing phase current as the speed increases. Hence, the instantaneous torque error compensation block increases the torque required from the incoming phase and the current is increased accordingly. This results in an overshoot on the incoming phase current.

The simulation results of the conventional cubic, proposed methods, in addition to the experimental result of the proposed method are compared and presented in Fig. 8.

A similar performance is achieved for both the cubic and proposed TSF methods at low speeds due to the low flux linkage derivation values; however, at higher speeds, the proposed method achieves lower torque ripple. The common problem of all the TSF methods is that the torque sharing gets harder as the speed increases; at some point, it becomes impossible to share the torque between consecutive phases with a mathematical expression after a certain speed limit. Here, the torque sharing in Cubic TSF can be performed up to 400 rpm within

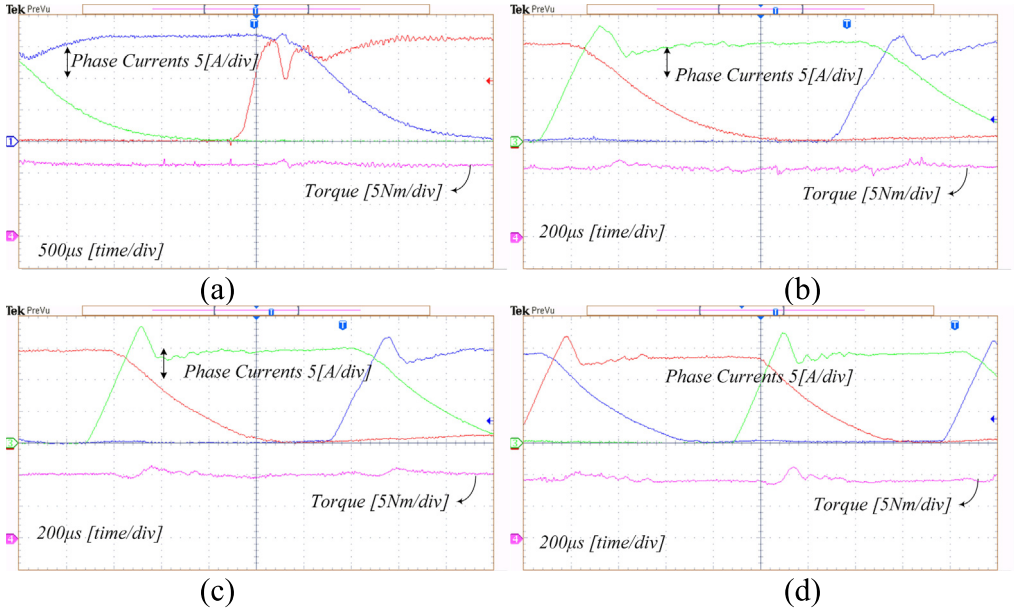

Fig. 7 Experimental result of the proposed method at (a) 400, (b) 1000, (c)1200, and 1400 rpm.

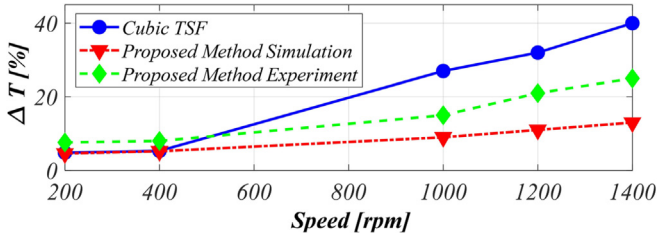

Fig. 8 Torque ripple versus speed comparison.

a 10% torque ripple limit while it can be performed up to 1000 rpm with the proposed method. Moreover, even after 1000 rpm, the torque ripple is significantly reduced thanks to the instantaneous torque estimation.

5. Conclusion

A torque sharing method based on instantaneous torque error compensation is presented. The aim is to benefit the torque generation from the outgoing phase as long as it is possible as its inductance is high and current dynamics are slow. A second-order LPF is used to determine the trajectory of the outgoing phase current. The LPF's cutoff frequency and turn-off angle are optimized to avoid negative torque generation and circulating currents while having the minimum torque ripple. The incoming phase is turned on at the earliest position where a positive torque can be produced. During this process, the torque is estimated instantaneously, and a correction current is calculated using LUTs and injected into the incoming phase current. This way, torque ripple is reduced for an extended speed range. Compared to the conventional TSF methods, torque sharing is not formulated with a mathematical expression. Instead, it is formed based on instantaneous torque error. As a result, the proposed TSF method can work at higher speed levels thanks to the adaptive commutation technique. The proposed method is simulated and experimentally verified. Compared to the conventional cubic TSF, the proposed controller performed similarly up to the base speed. However, the proposed method can operate at a higher speed level with a lower torque ripple.

Declaration of Competing Interest

The authors declare that they have no known competing financial interests or personal relationships that could have appeared to influence the work reported in this paper.

References

[1] R. Krishnan, Switched Reluctance Motor Drives: Modeling, Simulation, Analysis, Design, and Applications, CRC Press/Taylor & Francis Group, Boca Raton, FL, 2001. doi:10.1201/9781420041644.

[2] B. Bilgin, J.W. Jiang, A. Emadi, Switched Reluctance Motor Drivers, CRC Press/Taylor & Francis Group, Boca Raton (2019), https://doi.org/10.1201/9780203729991.

[3] Y. Yasa, D. Tekgun, Y. Sozer, J. Kutz, J. Tylenda, Effect of distributed airgap in the stator for acoustic noise reduction in switched reluctance motors, Conference Proceedings - IEEE Applied Power Electronics Conference and Exposition - APEC. (2017) 633–639. doi:10.1109/APEC.2017.7930760.

[4] T. Husain, Y. Sozer, I. Husain, DC-Assisted Bipolar Switched Reluctance Machine, IEEE Trans Ind Appl. 53 (2017) 2098–2109, https://doi.org/10.1109/TIA.2017.2675363.

[5] L. Al Quraan, Adaptive Firing Angles Control for Switched Reluctance Motor, (2023) 119–124.

[6] P. Bober, Online Optimization of Firing Angles for Switched Reluctance, Motor Control (2021) 3–7.

[7] G. Fang, F. Pinarello Scalcon, D. Xiao, R. Vieira, H. Grundling, A. Emadi, Advanced Control of Switched Reluctance Motors (SRMs): A Review on Current Regulation, Torque Control and Vibration Suppression, IEEE Open Journal of the Industrial Electronics, Society. 2 (2021) 280–301, https://doi.org/10.1109/ojies.2021.3076807.

[8] A. Xu, C. Shang, J. Chen, J. Zhu, L. Han, A New Control Method Based on DTC and MPC to Reduce Torque Ripple in SRM, IEEE Access. 7 (2019) 68584–68593, https://doi.org/10.1109/ACCESS.2019.2917317.

[9] S. Yao, W. Zhang, A Simple Strategy for Parameters Identification of SRM Direct Instantaneous Torque Control, IEEE Trans Power Electron. 33 (2018) 3622–3630, https://doi.org/10.1109/TPEL.2017.2710137.

[10] R. Mikail, Y. Sozer, I. Husain, M. Islam, T. Sebastian, Torque ripple minimization of switched reluctance machines through current profiling, IEEE Energy Conversion Congress and Exposition: Energy Conversion Innovation for a Clean Energy Future, ECCE 2011, Proceedings. (2011) 3568–3574. doi:10.1109/ECCE.2011.6064252.

[11] O. Boler, A.W. Bandarkar, NVH Performance of Direct Flux Controlled Switched Reluctance Machine (2020) 5771–5776.

[12] F. Al-Amyal, L. Al Quraan, L. Szamel, Torque Sharing Function Optimization for Extended Speed Range Control in Switched Reluctance Motor Drive, (2021) 000119–000124. doi:10.1109/cando-epe51100.2020.9337792.

[13] X.D. Xue, K.W.E. Cheng, S.L. Ho, Optimization and evaluation of torque-sharing functions for torque ripple minimization in switched reluctance motor drives, IEEE Trans Power Electron. 24 (2009) 2076–2090, https://doi.org/10.1109/TPEL.2009.2019581.

[14] J. Ye, B. Bilgin, A. Emadi, An Offline Torque Sharing Function for Torque Ripple Reduction in Switched Reluctance Motor Drives, IEEE Trans Energy Convers. 30 (2015) 726–735, https://doi.org/10.1109/TEC.2014.2383991.

[15] H. Li, B. Bilgin, A. Emadi, An Improved Torque Sharing Function for Torque Ripple Reduction in Switched Reluctance Machines, IEEE Trans Power Electron. 34 (2019) 1635–1644, https://doi.org/10.1109/TPEL.2018.2835773.

[16] Y. Wei, M. Qishuang, Z. Poming, G. Yangyang, Torque ripple reduction in switched reluctance motor using a novel torque sharing function, AUS 2016 - 2016 IEEE/CSAA International Conference on Aircraft Utility Systems. (2016) 177–182. doi:10.1109/AUS.2016.7748043.

[17] A.K. Rana, A.V.R. Teja, A Mathematical Torque Ripple Minimization Technique Based on Nonlinear Modulating Factor for Switched Reluctance Motor Drives, 0046 (2021). doi:10.1109/TIE.2021.3063871.

[18] Z. Xia, B. Bilgin, S. Nalakath, A. Emadi, A New Torque Sharing Function Method For Switched Reluctance Machines With Lower Current Tracking Error, IEEE Transactions on Industrial Electronics. 0046 (2020), https://doi.org/10.1109/TIE.2020.3037987.

[19] T.H. Kim, D.H. Lee, J.W. Ahn, Advanced non-linear logic torque sharing function of SRM for torque ripple reduction, INTELEC, International Telecommunications Energy Conference (Proceedings). (2009) 1–4. doi:10.1109/INTLEC.2009.5351818.

[20] X.D. Xue, K.W.E. Cheng, S.L. Ho, A control scheme of torque ripple minimization for SRM drives based on flux linkage controller and torque sharing function, 2006 2nd International Conference on Power Electronics Systems and Applications, ICPESA. (2006) 79–84. doi:10.1109/PESA.2006.343074.

[21] J. Ye, B. Bilgin, A. Emadi, An extended-speed low-ripple torque control of switched reluctance motor drives, IEEE Trans Power Electron. 30 (2015) 1457–1470, https://doi.org/10.1109/TPEL.2014.2316272.

[22] R. Harikrishnan, F.M. Fernandez, Improved online torque-sharing-function based low ripple torque control of switched reluctance motor drives, IEEE International Conference on Power Electronics, Drives and Energy Systems, PEDES 2016. 2016-Janua (2017) 1–6. doi:10.1109/PEDES.2016.7914374.

[23] R.B. Inderka, R.W.A.A. De Doncker, DITC - Direct Instantaneous Torque Control of Switched Reluctance Drives, IEEE Trans Ind Appl. 39 (2003) 1046–1051, https://doi.org/10.1109/TIA.2003.814578.
[24] I. Husain, M. Ehsani, Torque ripple minimization in switched reluctance motor drives by PWM current control, IEEE Trans Power Electron. 11 (1996) 83–88, https://doi.org/10.1109/63.484420.
[25] D. Tekgun, B. Tekgun, I. Alan, FEA based fast topology optimization method for switched reluctance machines, Electr Eng. 104 (2022) 1985–1995, https://doi.org/10.1007/s00202-021-01453-9.